AIAA JOURNAL
Vol. 38, No. 11, November 2000

Navier–Stokes Airfoil Computations with e^N Transition Prediction Including Transitional Flow Regions

Hans W. Stock*
DLR, German Aerospace Research Center, 38108 Brunswick, Germany
and
Werner Haase†
DaimlerChrysler Aerospace AG, 81663 Munich, Germany

The flow around laminar airfoils is computed using a Navier–Stokes method coupled to a transition prediction method based on the e^N approach. Applying point transition at the predicted transition location produces a strong viscous/inviscid interaction region that prevents the coupled system from converging, whereas the introduction of transitional flow regions resolves that problem. The emphasis is not placed on the development of new transitional flow models but primarily on producing convergence, applying modified, available models. A comprehensive computational study is performed in a strong adverse and zero pressure gradient airfoil flow region, as the transitional lengths differ considerably for the different models. A conventional model, which is applicable in flow regions where transition is predicted well upstream of laminar separation, is proposed, together with a special transitional length model for flows where the boundary layer stays laminar up to separation. The flows over the DoAL3 and the NLF(1)-0416 laminar airfoils are investigated. The coupled Navier–Stokes and e^N methods are shown to produce converged results. Furthermore, the values for lift and drag are in excellent agreement with the free transition measurements.

Nomenclature

C = chord length
C_D = total drag coefficient
C_f = skin friction coefficient, $\tau_w / \frac{1}{2}\rho_\infty U_\infty^2$
C_L = lift coefficient
C_p = pressure coefficient
H_i = kinematic shape parameter, δ_i^* / θ_i
k = von Kármán constant
M = freestream Mach number
Re = Reynolds number based on chord and freestream conditions
$Re_{X_{\mathrm{tr}}}$ = local Reynolds number based on X_{tr}
$Re_{\Delta X}$ = local Reynolds number based on ΔX
$Re_{\delta^*_{\mathrm{tr}}}$ = local Reynolds number based on the displacement thickness δ^* at transition
U = velocity component in wall parallel direction
U_τ = friction velocity, $(\tau_w / \rho_w)^{1/2}$
U^+ = dimensionless velocity, U / U_τ
X = coordinate in freestream direction
X_T = X value at the start of fully turbulent flow
X_{tr} = X value at transition
Y = wall normal coordinate
y^+ = dimensionless wall distance, YU_τ / ν
α = angle of attack
γ = intermittency
ΔX = length of the transitional flow regime
δ = boundary-layer thickness
δ^* = displacement thickness,

$$\int_0^\delta \left(1 - \frac{\rho U}{\rho_e U_e}\right) \mathrm{d}Y$$

δ_i^* = kinematic displacement thickness,

$$\int_0^\delta \left(1 - \frac{U}{U_e}\right) \mathrm{d}Y$$

ε = eddy viscosity
θ_i = kinematic momentum loss thickness,

$$\int_0^\delta \frac{U}{U_e}\left(1 - \frac{U}{U_e}\right) \mathrm{d}Y$$

ν = viscosity
ρ = density
Ψ = propagation direction angle of unstable perturbations, when equal to 0 is the direction aligned with the resultant velocity direction at the outer edge of the boundary layer

Subscripts

e = outer edge of the boundary layer
tr = transition

I. Introduction

LAMINAR flow technology has attracted a considerable interest over the last decade. Laminar regions on aircraft, that is, over large parts of the wings and nacelles, especially of high bypass ratio nacelles, will reduce the aircraft drag and thereby the fuel consumption enough to support the efforts fed into the laminar flow research. The range of activities covers fundamental research in laminar–turbulent transition, the development of design tools for laminar airfoils, wings, and nacelles, and includes transition prediction methods. Wind-tunnel and free-flight tests are undertaken on laminar gloves, either for natural laminar flow wings or for hybrid laminar flow wings and nacelles. For the latter, a suction panel is used to suppress premature transition.

The development of design tools is mostly concentrated on reliable transition prediction methods, the range of which extends from simple empirical relationships via stability theories of different levels (parallel flow and linear or nonlinear parabolized stability equation methods) to direct numerical simulations. The e^N method,[1,2]

Received 20 July 1999; revision received 28 March 2000; accepted for publication 2 May 2000.

*Senior Research Scientist, Institute of Design Aerodynamics, Lilienthalplatz 7.
†Senior Research Scientist, Flight Physics Department, Military Aircraft Division, P.O. Box 801160.

based on local, linear stability theory and the parallel flow assumption, still represents the current state of the art for transition onset prediction in the aircraft industry.[3–5] The idea of the e^N method goes back to Liepmann,[6] who hypothesized that, at the breakdown of laminar to transitional or turbulent boundary-layer flow, the maximum Reynolds stress $\tau_{\max} = -\rho\overline{u'v'}$ due to amplified fluctuations becomes comparable in magnitude to the maximum laminar shear stress. Smith and Gamberoni[1] and van Ingen[2] took over this hypothesis and computed the amplitude amplification of perturbations applying the local, linear stability theory. On one hand, transition mechanisms such as bypass and attachment line transition are excluded from this approach, similar to the problem of receptivity. On the other hand, transition due to the excitation of Tollmien–Schlichting and crossflow instabilities can be predicted (two N factor method).

The local, linear stability theory offers different strategies to be applied for the analysis of three-dimensional flows, that is, a compressible or incompressible analysis, the envelope method, the fixed frequency and constant propagation direction method, and the fixed frequency and constant total wavelength or constant spanwise wave number method with or without curvature effects. Overviews of the different strategies are given in Refs. 4, 5, 7, and 8. Based on the experience gained by analyzing wind-tunnel and free-flight test data, a clear preference for the two N factor e^N method is given to the strategy applying the incompressible analysis without curvature. Furthermore, the selected strategy uses fixed frequencies together with a propagation direction of $\Psi = 0$ deg for Tollmien–Schlichting waves and for crossflow instabilities standing waves, $f = 0$ Hz, together with constant total wavelength or constant spanwise wave number.

The value of e^N represents for a certain perturbation the ratio of its amplitude entering the unstable zone to that at the transition location. In this aspect, the e^N method is a semi-empirical approach because the two limiting N factors for Tollmien–Schlichting and crossflow instabilities at transition are not known a priori. In several wind-tunnel campaigns, the limiting N factors were determined for the S1MA transonic facility,[9,10] ONERA, Modane, France, the Dutch German low-speed tunnel (DNW), The Netherlands,[11] the transonic wind tunnel at the DLR, German Aerospace Research Center (TWB), Brunswick, Germany,[12] and the Royal Aerospace Establishment (RAE) Bedford tunnel,[13] England, United Kingdom. The analysis of free-flight test data at subsonic and transonic speeds on laminar wing gloves using as test bed the LFU-205 (Ref. 11), the Dornier Do228 (Refs. 14–16), the VFW-614 (Refs. 7, 9, and 17) (ATTAS program), the Fokker-100 (Refs. 4, 5, and 8) (ELFIN program), and on a nacelle[18,19] allowed the evaluation of the two limiting N factors to be used as stability boundaries in flight conditions. These stability boundaries were introduced in computational methods for the design of laminar gloves for the ATTAS wing,[20] the ELFIN wing,[21] the fin on the Airbus A320,[22] and the nacelle.[23,24]

The two N factor e^N method so far is applied in the design using coupled methods, that is, inviscid flow methods (panel, full potential, and Euler codes) and three-dimensional boundary-layer methods. Today, the demand for Navier–Stokes methods coupled to e^N transition prediction capabilities for the three-dimensional wing design clearly exists. Recently, in a first step, the problem of coupling Navier–Stokes codes for two-dimensional airfoil calculations with the e^N method has been tackled.[25–28]

Point transition is so far applied in Navier–Stokes codes, defined by merely switching on the turbulence model at transition onset. On one hand, this procedure results in an eddy viscosity production that yields rapid but not abrupt changes of the viscous layer properties; thus, a small transitional zone is created computationally.[28] On the other hand, point transition represents a local perturbation due to the relatively sharp reduction in the displacement thickness in the vicinity of transition, which produces a strong viscous/inviscid interaction region with a remarkable upstream influence. Considerable perturbations in wall pressure and in viscous layer properties are present, which prevent the iteratively coupled Navier–Stokes and e^N method computations to converge. To the contrary, the application of a finite length transitional zone in Navier–Stokes computations will be shown to reduce the strength of the local perturbation; correspondingly, the changes in wall pressure and viscous flow data will be more moderate.

Hence in the present paper, the subject of flow computations over airfoils is pursued, with main interest placed on the inclusion of transitional flow computations. The emphasis is not to develop novel transitional zone models, but primarily directed to convergence aspects of the coupled Navier–Stokes and e^N methods.

Note that for low Reynolds number airfoil flows transition may not occur before the laminar boundary layer separates. Conventionally, a laminar separation bubble will develop, where the laminar free shear layer becomes unstable and reattaches turbulently, or under certain circumstances, the bubble bursts, producing laminar stall. These complex flow situations are not investigated in the context of the present paper. For these cases, transition will be fixed just before laminar separation instead.

II. Transitional Flow Models

The transitional flow is usually considered to be characterized by the intermittent appearance of turbulent spots, which grow in the lateral and longitudinal directions as they move downstream and finally merge to form the fully turbulent flow. Only time-averaged values are considered for the turbulent intermittency. Furthermore, the intermittency is supposed to depend only on the wall parallel direction; the wall normal variation is neglected. This concept was first formulated by Emmons[29] and later verified by experiments of Schubauer and Klebanoff,[30] Elder,[31] and others.

All averaged flow properties vary smoothly from the laminar to the turbulent flow regime. Accordingly, the intermittency factor, defined as the fraction of time occupied by turbulent spots, increases from zero to unity through the transitional area. Dhawan and Narasimha[32] proposed a universal turbulent intermittency function, which is commonly accepted and successfully applied. The intermittency function γ is independent on the wall normal direction and the forcing agent of the transition process[32]:

$$\gamma = 1 - \exp[-0.411\xi^2] \tag{1}$$

where

$$\xi = (X - X_{\mathrm{tr}})/\lambda \tag{2}$$

$$X_{\mathrm{tr}} = X_{\gamma=0} \tag{3}$$

$$\lambda = X_{\gamma=0.75} - X_{\gamma=0.25} \tag{4}$$

Defining the downstream limit of the transitional zone as

$$X_T = X_{\gamma=0.99} \tag{5}$$

gives

$$\Delta X = X_T - X_{\mathrm{tr}} = 3.36\lambda \tag{6}$$

The longitudinal extension of the transitional flow regime ΔX can be described by the models of Narasimha,[33] Chen and Thyson,[34] and Walker.[35] The proposed formulations for ΔX are as follows for each reference.

Narasimha[33]:

$$Re_{\Delta X} = 30.2\, Re_{X_{\mathrm{tr}}}^{\frac{3}{4}} \tag{7}$$

Chen and Thyson[34]:

$$Re_{\Delta X} = \left[60 + 4.68 M_e^{1.92}\right] Re_{X_{\mathrm{tr}}}^{\frac{2}{3}} \tag{8}$$

Walker[35]:

$$Re_{\Delta X} = 5.2\, Re_{X_{\mathrm{tr}}}^{\frac{3}{4}} \tag{9}$$

These cited expressions originate from investigations of flat plate flows. To cope with pressure gradient flows, boundary-layer history effects are introduced, replacing the X coordinate at transition by a convenient boundary-layer property at transition. When using the displacement thickness as the scaling property, the incompressible flat plate Blasius flow gives

$$Re_{\delta^*_{\mathrm{tr}}} = 1.72\, Re_{X_{\mathrm{tr}}}^{\frac{1}{2}} \tag{10}$$

Rewriting Eqs. (7–9) and ignoring for now the compressibility term in Eq. (8) deliver the following modified relations.

Narasimha[33]:

$$Re_{\Delta X} = 13.4\, Re_{\delta^*_{tr}}^{\frac{3}{2}} \tag{11}$$

Chen and Thyson[34]:

$$Re_{\Delta X} = 29.1\, Re_{\delta^*_{tr}}^{\frac{4}{3}} \tag{12}$$

Walker[35]:

$$Re_{\Delta X} = 2.3\, Re_{\delta^*_{tr}}^{\frac{3}{2}} \tag{13}$$

The new set of equations for the transitional length [Eqs. (11–13)] requires the evaluation of the laminar boundary-layer thickness δ, which is not known a priori in Navier–Stokes methods. In Ref. 28 a procedure is described to compute δ and thereby δ^* for laminar flows. The eddy viscosity in the transitional region is defined as

$$\varepsilon_{\text{trans}} = \gamma \varepsilon \tag{14}$$

III. Applied Navier–Stokes Method

The Reynolds-averaged Navier–Stokes equations, describing two-dimensional, unsteady, compressible flows in conservation form, are solved by means of a finite volume approach using a Runge–Kutta time-stepping method with multigrid acceleration.[36] In the turbulent part of the viscous layer, the Johnson–King turbulence model is applied in its original form.[37]

All Navier–Stokes computations are carried out using four mesh levels for the multigrid procedure, with 512×128 mesh volumes in the finest grid. The grid indepence of the computational results is documented in Ref. 28. The computations are performed on adapted meshes, which ensure that in the wall normal direction a sufficiently large and moreover constant number of mesh points is embedded inside the viscous layer from the stagnation point to the airfoil trailing edge. The procedures to evaluate the viscous layer outer edge for Navier–Stokes computations are described in Ref. 28 for the laminar flow region and in Ref. 38 for the turbulent flow region. Conventionally, 60–65 mesh points are placed inside the viscous layer. Navier–Stokes data computed on viscous adapted meshes only are shown to be of boundary-layer computation quality.[28]

IV. Numerical Study of Transitional Flows

The DoAL3 laminar airfoil, developed at Dornier, is used first for the present numerical study. The measurements were performed in the TWB facility at the DLR, German Aerospace Research Establishment[39] at a Mach number of $M = 0.48$ and a Reynolds number of $Re = 3.2 \times 10^6$. The limiting N factor of that wind tunnel was determined beforehand for Tollmien–Schlichting waves to be $N = 6$ (Ref. 12).

Figure 1 shows two different pressure distributions for the angle of attack $\alpha = 2$ deg computed on adapted meshes. The solid line represents the pressure distribution of the first Navier–Stokes solution when point transition is imposed for the start just before laminar separation on both airfoil surfaces. The e^N method[40] in combination with the limiting N factor, $N = 6$, predicts transition at $X/C = 0.073$ on the upper surface. Transition on the lower surface remains fixed at $X/C = 0.685$ just before laminar separation because the computed N factors show values well below $N = 6$ up to laminar separation. The dotted line describes the results obtained for point transition of the second Navier–Stokes iteration. The global result is as expected; the lift is clearly reduced by shifting the transition location on the upper surface from $X/C = 0.611$ to 0.073. In detail, however, it can be seen clearly that the wall pressure distributions are distorted around the locations where point transition is introduced. As a consequence, the e^N computation using the upper surface data of the second Navier–Stokes iteration is no longer successful. The N factor value remained constantly well below $N = 6$ up to the location where transition is predicted by the first iteration. The reason for that failure is obviously due to the application of point transition, which is responsible for the perturbations in the viscous layer data and the wall pressure.

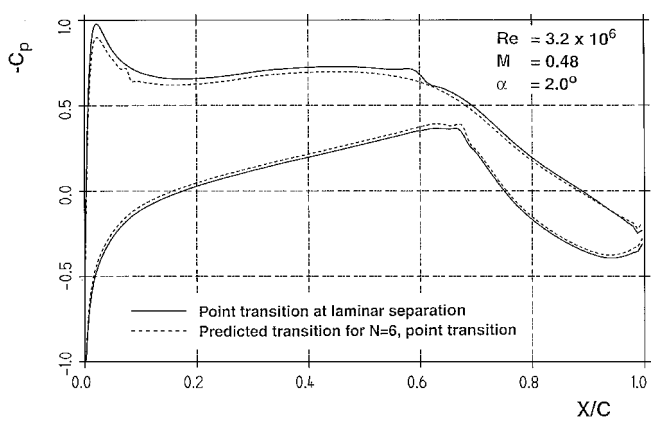

Fig. 1 Pressure distributions on the DoAL3 airfoil for the first Navier–Stokes iteration with transition fixed at laminar separation and for the second iteration with predicted transition using point transition.

A detailed investigation of transitional flow modeling in Navier–Stokes methods appears to be necessary as the earlier mentioned models deliver quite substantial differences, and, furthermore, previous publications on that topic could not be found in the literature.

A. Scatter of the Transitional Lengths Models

Based on the flow data of the first Navier–Stokes iteration, which are computed for point transition fixed just before laminar separation (Fig. 1), the derived values for the transitional lengths ΔX are presented in Fig. 2a as a function of X/C using the original models [Eqs. (7–9)] and the modified models [Eq. (11–13)]; negative values of X/C indicate the lower surface. It can be easily detected that the model of Narasimha[33] delivers values that are six times larger than the minimum length model of Walker,[35] and even the Chen and Thyson[34] expression produces values three times larger than the minimum length model.

The transitional lengths, evaluated with the modified relationships, are larger on the upper and smaller on the lower surface compared to the original model values due to the suction peak on the upper surface, which causes a more rapid growth of the boundary layer in the adverse pressure gradient region. In contrast, the boundary layer on the lower surface is thinner compared to a flat plate boundary layer due to the continously accelerated flow.

Figure 2b shows the Reynolds number distribution based on ΔX vs the Reynolds number based on the X coordinate at transition X_{tr}. The solid, dashed, and dotted lines represent the original models, whereas the symbols describe the corresponding values of the modified models for the upper and lower surfaces, respectively. Because of the smaller exponent in the Chen and Thyson[34] model, the difference to the minimum length model of Walker[35] is decreasing with increasing transition Reynolds number.

The scatter in the predicted transitional lengths based on the different models is such that the user is forced to make an ad hoc decision about which model can be applied. To support the decision, Navier–Stokes results that have been obtained are thoroughly investigated by applying varying transitional lengths in different pressure gradient regions.

On the upper surface of the DoAL3 airfoil, laminar flow separation occurs at $X/C = 0.611$ (Fig. 1). In between the stagnation and the separation points, the laminar flow undergoes a strong adverse pressure gradient in the region of $X/C = 0.08$ and a nearly zero pressure gradient around $X/C = 0.45$. In these two regions of interest, computations are performed applying transitional lengths from 0 to 20% chord.

B. Variable Transitional Length in the Adverse Pressure Gradient Region

For the first 20% chord, Figs. 3 show the pressure (Fig. 3a) and displacement thickness distribution (Fig. 3b) on the upper surface for different values of ΔX, with transition fixed in the strong adverse pressure gradient region at $X/C = 0.08$. For comparison, the solid lines show the results obtained for point transition fixed before laminar separation on the upper surface at $X/C = 0.611$. The wavelike perturbation in pressure for point transition $\Delta X = 0$ is clearly seen.

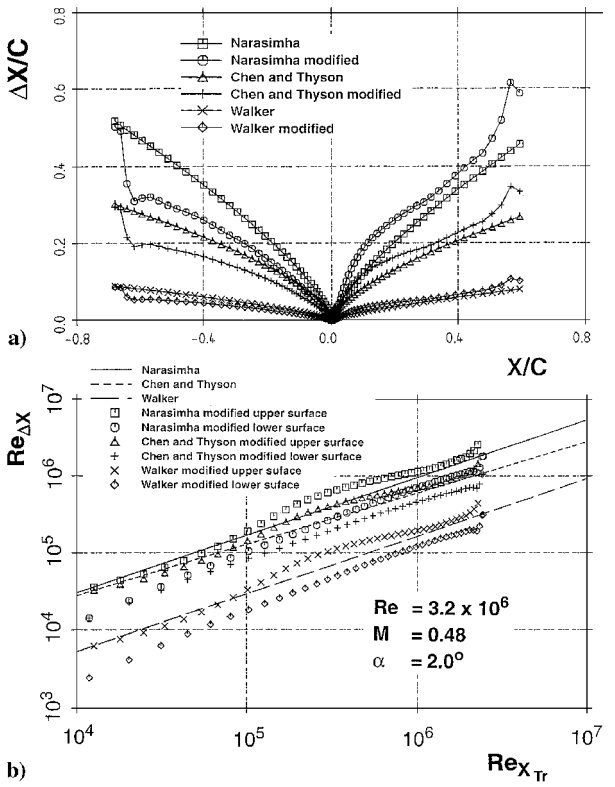

Fig. 2 Different models: a) transitional length ΔX and b) Reynolds number based on ΔX.

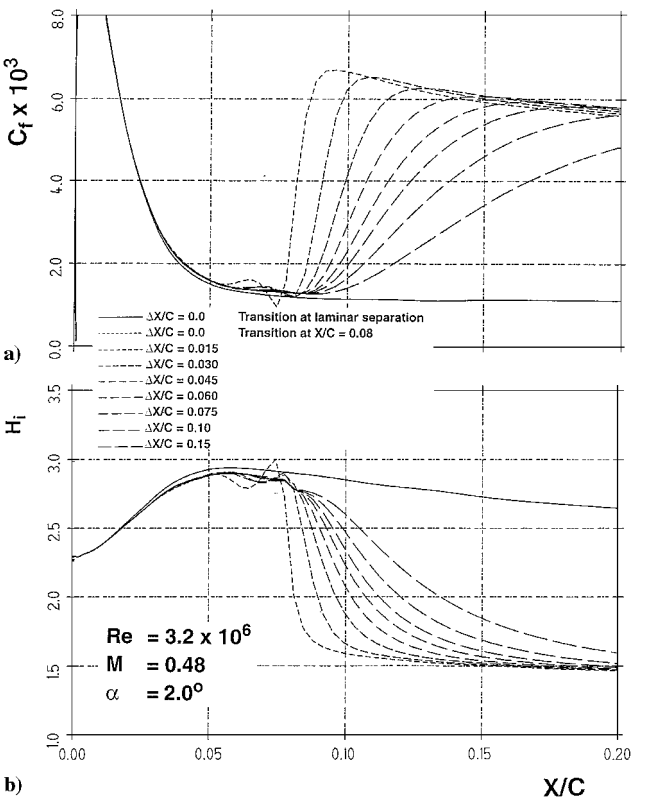

Fig. 4 Upper surface for different transitional lengths with fixed transition at $X/C = 0.08$: a) skin friction and b) shape parameter distribution.

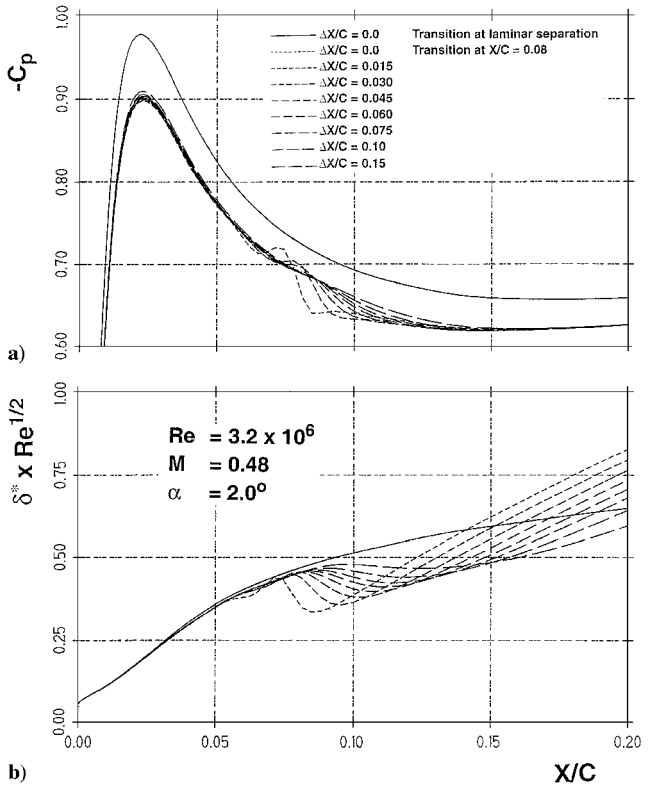

Fig. 3 Upper surface for different transitional lengths with fixed transition at $X/C = 0.08$: a) pressure and b) displacement thickness distribution.

Transition fixing at $X/C = 0.08$ reduces the suction peak in pressure as compared to the case where transition is imposed at $X/C = 0.611$; the boundary-layer is thickened considerably, the airfoil more decambered, the circulation lowered, and in turn the stagnation point is shifted on the lower surface upstream from $X/C = 0.928 \times 10^{-3}$ to 0.656×10^{-3}. A similar but in scale reduced behavior can be observed for the different transitional length computations. The maximum value of ΔX delivers the smallest value of the boundary-layer thickness downstream of the transitional zone, which results in the largest value for the suction peak pressure. The corresponding values for the skin friction C_f and the shape parameter H_i are given in Figs. 4a and 4b, respectively.

For all values of ΔX, the displacement thickness first decreases in the vicinity of transition, achieves a local minimum, and then continuously grows downstream. A neck region is formed in the displacement thickness as the momentum transfer to the near-wall flow is intensified by increased mixing of the intermittent turbulence, which results in fuller boundary-layer velocity profiles. With increasing values for ΔX, the neck region becomes less pronounced, that is, the perturbations in pressure gradually decay and finally disappear completely for a value of $\Delta X = 0.15$. Simultaneously, the upstream influence is clearly reduced for increasing values of ΔX.

Figures 5a–5c show velocity profiles in nondimensional form U^+ as a function of y^+, for three different values of $\Delta X/C$, at eight X/C stations, starting at $X/C = 0.0743$ in the laminar flow region. Fully turbulent profiles are achieved at $X/C = 0.1336, 0.1852$, and 0.2481 for values of $\Delta X/C = 0.0$, 0.075, and 0.15, respectively. Although the increased transitional length shifts the position downstream, where fully turbulent flow is achieved, the overall behavior is very similar and the development to fully turbulent flow is regular in all cases. The most downstream velocity profiles, shown in Fig. 5, clearly obey the law of the wall

$$U^+ = (1/k)\ln y^+ + \text{const} \tag{15}$$

which is shown for comparison as the dashed line.

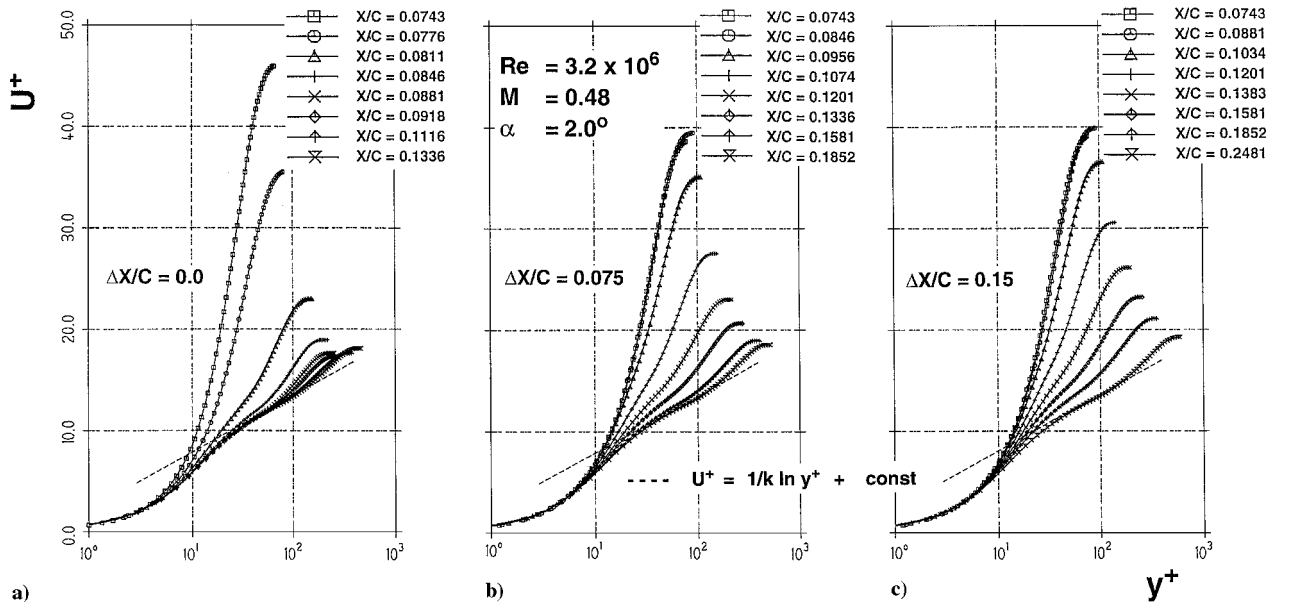

Fig. 5 Upper surface velocity profiles with fixed transition at $X/C = 0.08$ in the transitional zone for different transitional lengths: a) $\Delta X = 0.0$, b) $\Delta X = 0.075$, and c) $\Delta X = 0.15$.

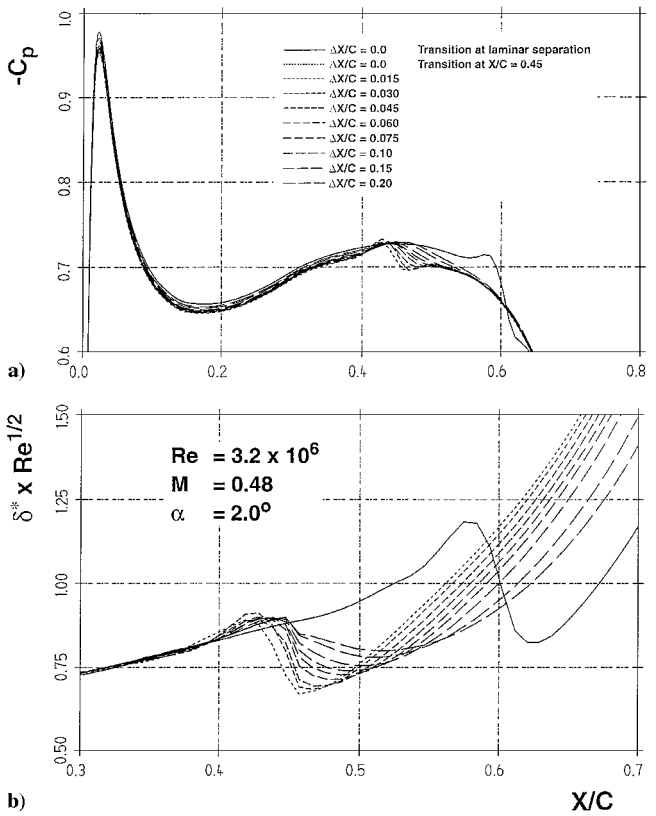

Fig. 6 Upper surface for different transitional lengths with transition fixed at $X/C = 0.45$: a) pressure and b) displacement thickness distribution.

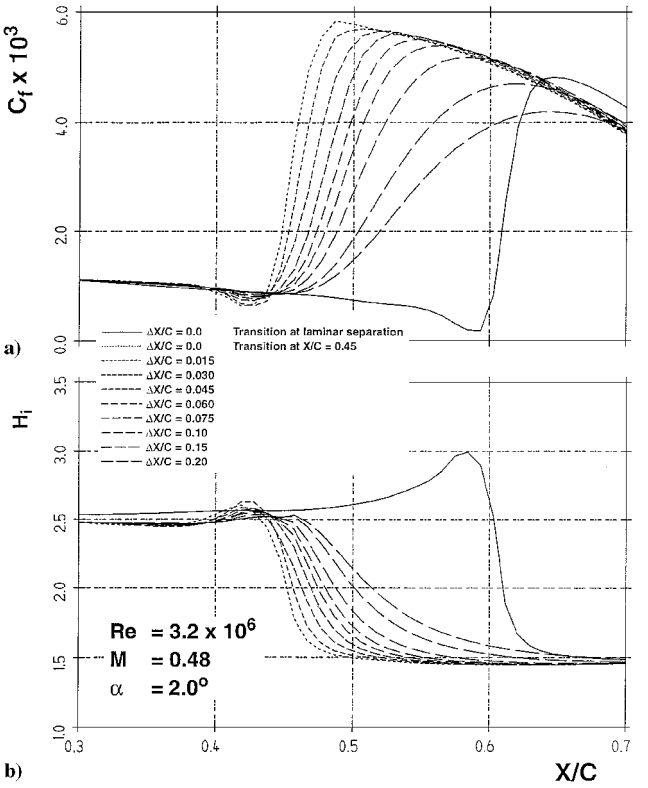

Fig. 7 Upper surface for different transitional lengths with transition fixed at $X/C = 0.45$: a) skin friction and b) shape parameter distribution.

C. Variable Transitional Length in the Zero Pressure Gradient Region

The second region of interest for fixing transition is at $X/C = 0.45$ on the upper surface of the airfoil, a region where the pressure gradient is nearly zero (Fig. 1). The computational results for the pressure and the displacement thickness distribution for ΔX values ranging from 0 up to 20% chord are shown in Figs. 6a and 6b together with those results that have been obtained for point transition at $X/C = 0.611$. The skin friction C_f and the shape parameter H_i are given in Figs. 7a and 7b, respectively. As it can be seen by comparing these results with the latter ones, neither a significant nor a systematic difference can be detected where transition was applied in the adverse pressure gradient region. However, the upstream influence is far more pronounced in the current case due to the larger boundary-layer thickness.

The variation of the displacement thickness $\Delta\delta^*$ is characterized by the difference between the maximum of δ^* upstream of transition and the minimum value of δ^* in the transitional zone. For point transition, the perturbation of the displacement thickness is $\Delta\delta^* Re^{1/2} = 0.227$, exhibiting about twice the value compared to the adverse pressure gradient case, where $\Delta\delta^* Re^{1/2} = 0.103$ (Fig. 3b).

On the other hand, the relative variations $\Delta\delta^*/\delta^*_{tr}$ are almost equal, $\Delta\delta^*/\delta^*_{tr} = 0.251$ and 0.238 for the zero and adverse pressure gradient cases, respectively.

V. Proposed Transitional Length Models

A. Conventional Transitional Length Model

Walker[35] states that the model given by Narasimha[33] clearly overestimates the transitional length. However, Walker's[35] transitional length model is based on restrictive assumptions, such that the estimate is considered to represent the minimum length. Walker[35] proposes to use the double value of the minimum length model, which is a clear ad hoc decision, but which represents a pragmatic compromise. By the following of this suggestion and also the considering of the numerical results discussed earlier, where transitional lengths up to 20% chord are applied without any obvious difficulty, the conventional transitional length model is proposed to be

$$Re_{\Delta X} = 10.4\, Re^{\frac{3}{4}}_{X_{tr}} \tag{16}$$

or in the modified version

$$Re_{\Delta X} = 4.6\, Re^{\frac{3}{2}}_{\delta^*_{tr}} \tag{17}$$

The conventional transitional length model is only applicable for flow situations where transition is predicted well upstream of laminar separation.

B. Special Transitional Length Model

On the lower surface of the DoAl3 airfoil, laminar separation takes place $X/C = 0.685$. Up to this position, all N curves show values well below the limiting N factor of $N = 6$. In the case of point transition, the viscous layer in the Navier–Stokes computation is able to overcome the adverse pressure gradient without separation due to the intense turbulent mixing. In contrast, transitional flow computations applying the conventional transitional length model produces large separated flow regions. For such cases, the convergence of the Navier–Stokes method to a steady state is no longer achievable. To overcome this problem, either the transition location can be shifted upstream or the transitional length can be reduced with respect to the values of Eqs. (16) or (17).

Laminar flow separation on airfoils conventionally takes place either downstream of the suction peak, where the adverse pressure gradient is large influencing a relative thin boundary layer, or farther downstream on the airfoil in the recompression region, where the adverse pressure gradient is milder but acting on a relative thick boundary layer. In both situations, the process of laminar–turbulent transition is believed to develop rapidly, clearly supporting the actual decision to maintain the transition location and, instead, to reduce the transitional length.

Based on numerical experiments, the result is that a good estimate for the special transitional length is the minimum length model of Walker[35] [Eqs. (9) and (13)]. The computations produce mostly attached flows or in some cases small separation bubbles, but stable solutions are achieved for all cases considered.

VI. Navier–Stokes and e^N Coupling Procedure

The viscous layer data of the first Navier–Stokes iteration with point transition fixed just before laminar separation on both airfoil surfaces are analyzed with the e^N method[40] in combination with the limiting N factor to determine the transition location. The transition locations are transferred in a slightly underrelaxed manner to the second Navier–Stokes iteration, where transitional zone computations are included. Usually three to four iteration cycles are now sufficient to produce a converged solution of the coupled system.

VII. Final Results

For validation purposes, the laminar DoAl3 (Ref. 39) and NLF(1)-0416 (Ref. 41) airfoils are selected, which are designed following different philosophies. The DoAL3 laminar airfoil is a test design for a laminar wing, which should produce in the Mach number range,

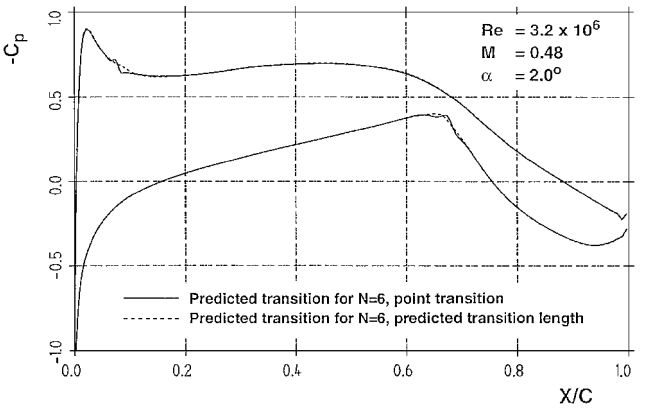

Fig. 8 Pressure distributions on the DoAL3 airfoil for the second Navier–Stokes iteration with predicted transition using point transition and for the last Navier–Stokes iteration with predicted transition and transitional flow.

$M = 0.45$–0.6, and for Reynolds numbers up to 12×10^6 laminar flow on upper and lower lower surface up to chordwise values of $X/C = 0.6$. Furthermore, the laminar bucket with a constant low drag value has to cover a large lift range because laminar flow is requested in cruise as well as in climb and descent. The low-speed NLF(1)-0416 laminar airfoil, however, is designed for high maximum lift for which minimum drag is not required to be constant above a certain value of lift and low drag is not required below cruise lift.

It is shown in Ref. 41 that the transition point on the upper surface of the NLF(1)-0416 laminar airfoil moves steadily toward the leading edge with increasing angle of attack, as opposed to the sudden jump characteristic on both surfaces of the DoAL3 airfoil. The limiting N factor for Tollmien–Schlichting waves for the NLF(1)-0416 laminar airfoil experiments was determined to be $N = 11$ (Ref. 42), based on transition location measurements.[41]

Figure 8 shows two different pressure distributions on the DoAl3 laminar airfoil for the angle of attack $\alpha = 2$ deg, similar to Fig. 1. The solid line represents the pressure distribution of the second Navier–Stokes iteration with transition predicted at $X/C = 0.073$ on the upper surface and before laminar separation on the lower surface using point transition. The dotted line describes the final result of the last Navier–Stokes iteration including transitional flow computations and transition predicted at $X/C = 0.08$ on the upper surface and before laminar separation on the lower surface. As may be seen, the perturbations in wall pressure are now nearly completely removed due to the inclusion of the transitional zone computation.

Figures 9a and 9b show the computed polars of the DoAL3 laminar airfoil compared to the measurements in the TWB facility.[39] The solid lines represent the results obtained for point transition fixed just before laminar separation. The maximum lift is predicted reasonably well, whereas the value of $dc_L/d\alpha$ is clearly overpredicted. This is because the tunnel walls of the TWB are slotted and the openings appear to be too large.[43] The drag, especially the minimum drag, is predicted well; apart from that, the extent of the laminar bucket is by far overpredicted. The reason is that transition fixing just before laminar separation overestimates the extent of laminarity on the airfoil in that wind tunnel. The solid circular symbols describe for $\alpha = -2$, -1, 0.8, and 2 deg the final result for predicted transition location with a limiting N factor, $N = 6$ (Ref. 12), and predicted transitional length. The lift is slightly reduced, due to the larger extent of turbulent flow. The computed drag nearly doubles for angles of attack $\alpha = -2$ and 2 deg, which is in good agreement with the experimentally observed values, and the extent of the laminar bucket is clearly reduced. The drag values for angles of attack $\alpha = -1$ and 0.8 deg are slightly lower compared to the values represented by the solid line due to the reduced skin friction in the transitional zones on both airfoil surfaces.

Finally, Figs. 10a and 10b show the computed polars of the NLF(1)-0416 laminar airfoil compared to the measurements in the low speed NASA Langley Research Center Low-Turbulence Pressure Tunnel (LTPT)[41] at a Mach number of $M = 0.1$ and a Reynolds

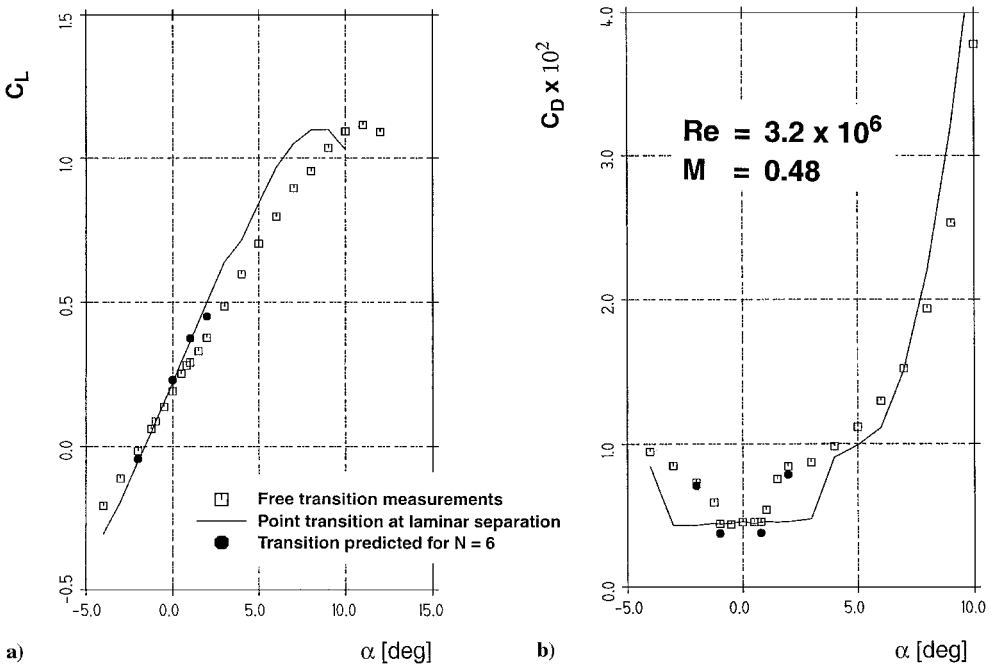

Fig. 9 DoAl3 airfoil for point transition at laminar separation and for predicted transition and transitional flow compared to measurements: a) lift and b) drag polar.

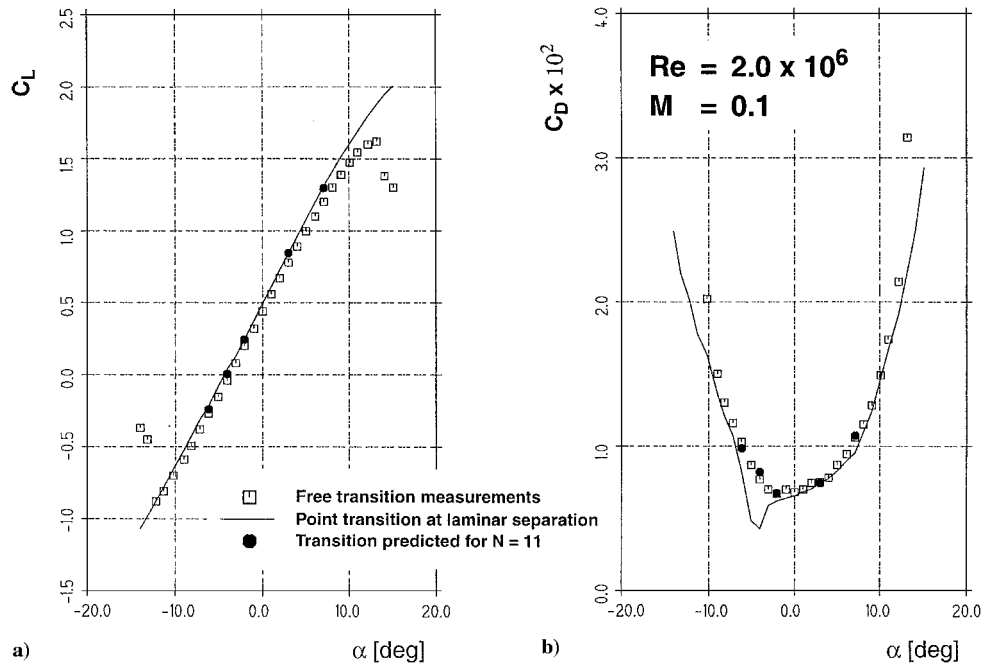

Fig. 10 NLF(1)-0416 airfoil for point transition at laminar separation and for predicted transition and transitional flow compared to measurements: a) lift and b) drag polar.

number of $Re = 2.0 \times 10^6$. The solid lines are the results obtained for point transition fixed just before laminar separation. In the range of angles of attack from $\alpha = -7$ up to $\alpha = -4$ deg, the peculiar behavior in drag is because of the extent of overprediction of the laminar flow region on both airfoil surfaces. The solid circular symbols describe the final results for predicted transition location with a limiting N factor, N = 11 (Ref. 42), and predicted transition length. The values of lift and drag are in excellent agreement with the experimental findings.

VIII. Conclusions

It is shown that reliable computations of transitional flows on airfoils can be generated by Navier–Stokes methods coupled to the e^N transition prediction. Furthermore, it is documented that convergence problems of the coupled system applying point transition are avoided by the introduction of transitional flow computations. The classical intermittency function is successfully applied in the Navier–Stokes method for the description of the flow region between the fully laminar and fully turbulent regime. A conventional transitional length model is proposed for flow situations where transition is predicted well upstream of laminar separation. Alternatively, if transition is not predicted up to laminar separation, mostly in low Reynolds number flows, transition is fixed just before laminar separation, ignoring the complex flow situation of laminar separation bubbles. The conventional transitional length model does not produce stable Navier–Stokes solutions for this case, whereas the proposed special transition length model results in stable solutions for all investigated cases.

The procedure is successfully applied to the DoAL3 and the NLF(1)-0416 laminar airfoils, which are measured in the TWB

facility at the DLR, German Aerospace Research Center, and in the low-speed LTPT, respectively. The computed values for lift and drag are shown to be in excellent agreement with the measurements.

Acknowledgments

This research has been supported in part by the European Commission in the EUROTRANS program in BRITE/EURAM (Basic Research for Industrial Technologies/European Research in Advanced Materials).

References

[1]Smith, A. M. O., and Gamberoni, N., "Transition, Pressure Gradient and Stability Theory," Douglas Aircraft Co., Rept. ES 26388, Long Beach, CA, 1956.

[2]van Ingen, J. L., "A Suggested Semi-Empirical Method for the Calculation of the Boundary Layer Transition Region," Dept. of Aerospace Engineering, Rept. VTH-74, Univ. of Delft, Delft, The Netherlands, 1956.

[3]Collier, F. S.,"Recent Progress in the Development of Laminar Aircraft," International Council of the Aeronautical Sciences, ICAS Paper 94-4.7.1, 1994.

[4]Schrauf, G., Perraud, J., and Lam, F., "Comparison of Boundary Layer Transition Predictions Using Free Flight Test Data," *Journal of Aircraft*, Vol. 35, No. 6, 1998, pp. 891–897.

[5]Schrauf, G., "Linear Stability Theory Applied to Wind Tunnel and Flight Experiments," *Proceedings of the 4th European Computational Conference, ECCOMAS 98*, Vol. 2, Wiley, Chichester, England, U.K., 1998, pp. 126–131.

[6]Liepmann, H. W., "Investigation of Boundary Layer Transition on Concave Walls," NACA ACR 4J28, 1945.

[7]Schrauf, G., "Transition Prediction Using Different Linear Stability Analysis Strategies," AIAA Paper 94-1848, 1994.

[8]Schrauf, G., Perraud, J., Lam, F., Stock, H. W., Vitiello, D., and Abbas, A., "Transition Prediction with Linear Stability Theory—Lessons Learned from the ELFIN F100 Flight Demonstrator," *2nd European Forum on Laminar Flow Technology*, Association Aeronautique et Astronautique de France, 1996, Paper 8.5.

[9]Henke, R., and Münch, F. X., "Natural Laminar Flow: A Wind Tunnel Test Campaign and Comparison with Free Flight Test Data," AIAA Paper 90-3045, 1990.

[10]Schmitt, V., Quast, A., and Hinsinger, R., "Wind Tunnel Investigation of the A320 Laminar Fin," *2nd European Forum on Laminar Flow Technology*, Association Aeronautique et Astronautique de France, 1996, Paper 5.2.

[11]Horstmann, K. H., Quast, A., and Redeker, G., "Flight and Wind Tunnel Investigations on Boundary Layer Transition," *Journal of Aircaft*, Vol. 27, No. 2, 1990, pp. 146–150.

[12]Köster, H., and Müller, R., "Bestimmung des N-Faktors im Transsonischen Windkanal Braunschweig (TWB) anhand von Druckverteilungs- und Umschlagspunktmessungen und dem Sally-Verfahren," *6th DGLR-Fach-Symposium (Strömungen mit Ablösung)*, DGLR-Rept. 88-05, Deutsche Gesellschaft für Luft- und Raumfahrt e.V., Bonn, 1988, pp. 77–92.

[13]Gaudet, L., Betts, C. J., and Ashill, P. R., "Experimental Investigation of Boundary Layer Transition on a Natural Laminar Flow Airfoil," *1st European Forum on Laminar Flow Technology*, DGLR-Bericht 92-06, Deutsche Gesellschaft für Luft- und Raumfahrt e.V., Bonn, 1992, pp. 132–140.

[14]Horstmann, K. H., and Körner, H., "Natural Laminar Flight Test Investigation for Commuter Aircraft Application," *2nd European Forum on Laminar Flow Technology*, Association Aeronautique et Astronautique de France, 1996, Paper 2.3.

[15]Horstmann, K. H., Müller, R., Dick, P., and Wohlrath, W., "Flugversuche am Laminarhandschuh der Do 228," Deutsche Gesellschaft für Luft- und Raumfahrt, DGLR-Bericht 92-07, Nov. 1992.

[16]Wohlrath, W., Echtle, H., Dick, P., Welte, D., Stock, H. W., Moeken, B., Horstmann, K. H., Müller, R., Rohardt, C. H., and Quast, A., "Design and Flight Test Evaluation of a Laminar Wing Glove on a Commuter Aircraft," International Council of the Aeronautical Sciences, ICAS Paper 94-5.4.1, 1994.

[17]Horstmann, K. H., Redeker, G., Quast, A., Dressler, U., and Bieler, H., "Flight Tests with a Natural Laminar Flow Glove on a Transport Aircraft," AIAA Paper 90-3044, 1990.

[18]Mullender, A. J., and Riedel, H., "A Laminar Flow Nacelle Flight Test Programme," *2nd European Forum on Laminar Flow Technology*, Association Aeronautique et Astronautique de France, 1996, Paper 2.4.

[19]Riedel, H., Horstmann, K. H., Ronzheimer, A., and Sitzmann, M., "Aerodynamic Design of a Natural Laminar Flow Nacelle and the Design Validation by Flight Testing," *Aerospace Science and Technology*, Vol. 1, No. 1, 1998, pp. 1–12.

[20]Redeker, G., Horstmann, K. H., Köster, H., Thiede, P., and Szodruch, J., "Design of a Natural Laminar Flow Glove for a Transport Aircraft," AIAA Paper 90-3043, 1990.

[21]Dressler, U., Hansen, H., Rill, S., Horstmann, K. H., Rohardt, C. H., and Wichmann, G., "Design of the Fokker F100 Natural Laminar Flow Glove," *1st European Forum on Laminar Flow Technology*, DGLR-Bericht 92-06, Deutsche Gesellschaft für Luft- und Raumfahrt, Bonn, 1992, pp. 152–163.

[22]Stuke, H., Preist, J., and Capbern, P., "Principles of Aerodynamic Layout and Design of a Demonstrator Suction System," *2nd European Forum on Laminar Flow Technology*, Association Aeronautique et Astronautique de France, 1996, Paper 6.4.

[23]Mullender, A. J., Lecordix, J. L., Lecossais, E., Godard, J. L., and Hepperle, M., "The ELFIN II and LARA HLF Nacelles: Design, Manufacture and Test," *2nd European Forum on Laminar Flow Technology*, Association Aeronautique et Astronautique de France, 1996, Paper 5.3.

[24]Radespiel, R., Horstmann, K. H., and Redeker, G., "Feasibility Study on the Design of a Laminar Flow Nacelle," *Journal of Aircraft*, Vol. 27, No. 11, 1990, pp. 959–965.

[25]Radespiel, R., Graage, K., and Brodersen, O., "Transition Predictions Using Reynolds-Averaged Navier–Stokes and Linear Stability Analysis Methods," AIAA Paper 91-1641, 1991.

[26]Garriz, J. A., Vatsa, V. N., and Sanetrik, M. D., "Issues Involved in Coupling Navier–Stokes Mean-Flow and Linear Stability Codes," AIAA Paper 94-0304, 1994.

[27]Ramakrishnan, R., Vatsa, V. N., Otto, J., and Kumar, A., "A Detailed Study of Mean-Flow Solutions for Stability Analysis of Transitional Flow," AIAA Paper 93-3052, 1993.

[28]Stock, H. W., and Haase, W., "A Feasibilty Study of e^N Transition Prediction in Navier–Stokes Methods for Airfoils," *AIAA Journal*, Vol. 37, No. 10, 1999, pp. 1187–1196.

[29]Emmons, H. W., "The Laminar-Turbulent Transition in a Boundary-Layer–Part I," *Journal of the Aeronautical Sciences*, Vol. 18, No. 7, 1951, pp. 490–498.

[30]Schubauer, G. B., and Klebanoff, P. S., "Contributionson the Mechanics of Boundary-Layer Transition," NACA Rept. 1289, 1955.

[31]Elder, J., "An Experimental Investigation of Turbulent Spots and Breakdown to Turbulence," *Journal of Fluid Mechanics*, Vol. 9, 1960, pp. 235–246.

[32]Dhawan, S., and Narasimha, R., "Some Properties of Boundary-Layer Flow During the Transition from Laminar to Turbulent Motion," *Journal of Fluid Mechanics*, Vol. 3, 1958, pp. 418–436.

[33]Narasimha, R., "A Note on Certain Turbulent Spot and Burst Frequencies," Dept. of Aeronautical Engineering, Rept. 78 FM 10, Indian Inst. of Science, Bangalore, India, 1978.

[34]Chen, K. K., and Thyson, N. A., "Extension of Emmon's Spot Theory to Flows on Blunt Bodies," *AIAA Journal*, Vol. 9, No. 5, 1971, pp. 821–825.

[35]Walker, G. J., "Transitional Flow on Axial Turbomachine Blading," *AIAA Journal*, Vol. 27, No. 5, 1989, pp. 595–602.

[36]Haase, W., "EUROVAL—A European Initiative on Validation of CFD Codes," *Notes on Numerical Fluid Mechanics*, Vol. 42, Vieweg, Brunswick, Germany, 1992, pp. 82–87.

[37]Johnson, D. A., and King, L. S., "A Mathematical Simple Turbulence Closure Model for Attached and Separated Turbulent-Boundary Layers," *AIAA Journal*, Vol. 23, No. 11, 1985, pp. 1684–1692.

[38]Stock, H. W., and Haase, W., "Determination of Length Scales in Algebraic Turbulence Models for Navier–Stokes Methods," *AIAA Journal*, Vol. 27, No. 1, 1989, pp. 5–14.

[39]Müller, R., Puffert-Meißner, W., and Lück, H., "Messungen am Laminarprofil DoAL3 im Transsonischen Windkanal Braunschweig (TWB)," DLR-Interner Bericht, Rept. IB 129-87/9, DLR, German Aerospace Research Center, Brunswick, Germany, 1987.

[40]Schrauf, G., "An Efficient Solver of the Eigenvalue Problem of the Linear Stability Equations for Three-Dimensional, Compressible Boundary Layer Flows," *6th DGLR-Fach-Symposium (Strömungen mit Ablösung)*, DGLR-Rept. 88-05, Deutsche Gesellschaft für Luft- und Raumfahrt, Bonn, 1988, pp. 18–27.

[41]Somers, D. M., "Design and Experimental Results for a Natural-Laminar-Flow Airfoil for General Aviation Applications," NASA TP 1861, 1981.

[42]Stock, H. W., "Navier–Stokes Computations of Laminar Airfoils Using e^N Transition Prediction," *DLR-Interner Bericht*, Rept. IB 129-99/18, DLR, German Aerospace Research Center, Brunswick, Germany, 1999.

[43]"Two-Dimensional Transonic Testing Methods," Final Rept. Garteur Action Group AD (AG-02), National Aerospace Lab., Rept. NLR TR 83086 L, Amsterdam, 1981.

R. M. C. So
Associate Editor